

RSC Advances



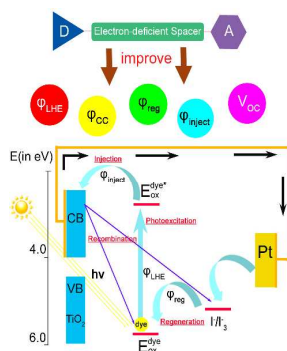
This is an *Accepted Manuscript*, which has been through the Royal Society of Chemistry peer review process and has been accepted for publication.

Accepted Manuscripts are published online shortly after acceptance, before technical editing, formatting and proof reading. Using this free service, authors can make their results available to the community, in citable form, before we publish the edited article. This *Accepted Manuscript* will be replaced by the edited, formatted and paginated article as soon as this is available.

You can find more information about *Accepted Manuscripts* in the [Information for Authors](#).

Please note that technical editing may introduce minor changes to the text and/or graphics, which may alter content. The journal's standard [Terms & Conditions](#) and the [Ethical guidelines](#) still apply. In no event shall the Royal Society of Chemistry be held responsible for any errors or omissions in this *Accepted Manuscript* or any consequences arising from the use of any information it contains.

The five important parameters (ϕ_{LHE} , ϕ_{inject} , ϕ_{reg} , ϕ_{cc} , V_{oc}) for DSSCs are improved by modifying the dyes with electron-deficient units.



Cite this: DOI: 10.1039/c0xx00000x

www.rsc.org/xxxxxx

PAPER

Exploring Photophysical Properties of Metal-free Coumarin Sensitizers: An Efficient Strategy to Improve Performance of Dye-sensitized Solar

Jinghui Wang,^a Ming Li,^{a, b} Dan Qi,^a Wei Shen,^a Rongxing He^{*a, b} and Sheng Hsien Lin^c

Received (in XXX, XXX) Xth XXXXXXXXX 20XX, Accepted Xth XXXXXXXXX 20XX

DOI: 10.1039/b000000x

An efficient strategy was provided by adopting different number of electron-deficient units (pyrimidyl and quinoly) into parent coumarin sensitizers to obtain excellent absorption in short-wavelength region (B2 band), which eventually improves the performance of DSSCs. Density functional theory calculations were performed on both free dyes and dye/TiO₂ complexes. As expected, introducing single electron-deficient unit results in a positive influence on power conversion efficiency (η) of DSSCs because of the larger short-circuit current density (J_{sc} is proportional to optical absorption (ϕ_{LHE}), charge separation, dye regeneration (ϕ_{reg}) and electron injection (ϕ_{inject})) and the higher open circuit voltage (V_{oc}). The introduction of more pyrimidine facilitates charge separation and favors effective electron injection, whereas the second quinoline displays opposite effect. The results give a guidance to design promising candidates for the future DSSCs applications.

1. Introduction

Dye-sensitized solar cells (DSSCs) have received immense attention due to high power conversion efficiency (η) and low cost as compared to conventional silicon-based solar cells.¹⁻³ So far Ru complexes are one of most promising dyes for DSSCs with $\eta > 11\%$, but the usage of rare and expensive ruthenium severely limits their application.² Therefore, metal-free organic dyes (facile molecular design and high molar extinction coefficient) are now being proposed to be an alternative of Ru-based sensitizers because they are cheaper, more abundant and less toxic.⁴⁻⁶

Coumarin 343 (C343) and its derivatives^{2, 7, 8} are one of the most promising families of organic dyes because they undergo efficient and fast electron injection successfully used in DSSCs, but their performance is limited by narrow photoresponse range in the whole visible region, unwelcome π -stacked aggregation and undesirable charge recombination.^{9, 10} For these reasons, the η of DSSCs using coumarin sensitizers is much lower than that based on Ru and Zn complexes.¹¹ Therefore, Hara *et al*¹² expanded the π -conjugation by inserting more vinylene units (-CH=CH-) or π -conjugated rings^{13, 14} (such as thiophene, benzene, furan or pyrrole) into the π -spacers and Rociosa *et al*¹⁵ introduced -NH₂ group into skeleton of coumarin to solve these problems. Despite these two strategies are helpful to broaden the absorption bands of coumarin sensitizers in long-wavelength region (Q band), the relatively weak and narrow absorption bands in short-wavelength region still severely attenuated the light capture capability of sensitizers and further restrict the efficiency of DSSCs.^{2, 16} How to put forward appropriate countermeasures to improve the absorption properties (including the absorption range and light harvesting efficiency) in the whole visible region has

become a topic much worthy of discussion. In this work, thus, different electron-deficient units were incorporated into π -spacers of dyes to improve the absorption intensity and broaden the absorption range of coumarin sensitizers in short-wavelength region. Experimentally, Wong *et al*¹⁷ testified that the triphenylamine-based sensitizers bearing a pyrimidine unit display enhanced spectral responses in the red portion of the solar spectrum and exhibit high η . Subsequently, He *et al*¹⁸ theoretically explored how the electron-deficient pyrimidine affected the performance of the porphyrin sensitizers, and clarified that the electron-deficient units would lead to redshift absorption and efficient charge separation. Most recently, He *et al*¹⁹ further investigated the role of varied-length spacers in electron transfer, especially the influence of π -spacer modified by electron-deficient units on electron transfer. They found that electron injection driving force of model compounds gradually decreases as the increase of π -spacer length, whereas the introduction of electron-deficient pyrimidinyl breaks the dependence of π -bridge length. With all the information, we believe that the adoption of electron-deficient units into the π -spacer is a feasible strategy to improve η of DSSCs. On the basis of the theoretical interpretation together with the experimental results, two questions are worthy of considering. Firstly, it is found that the performance of DSSCs is improved when electron-deficient unit is adopted in π -bridge of metal organic dyes. So we are very curious to know whether the metal-free coumarin sensitizers that introduce electron-deficient units can also improve the light-harvesting efficiency and further raise the performance of DSSCs. Secondly, how do the different electron-deficient units and their amount influence absorption spectra, intrinsic characters of electron transition and different electron transfer processes of free sensitizers? It is not sufficient to assess

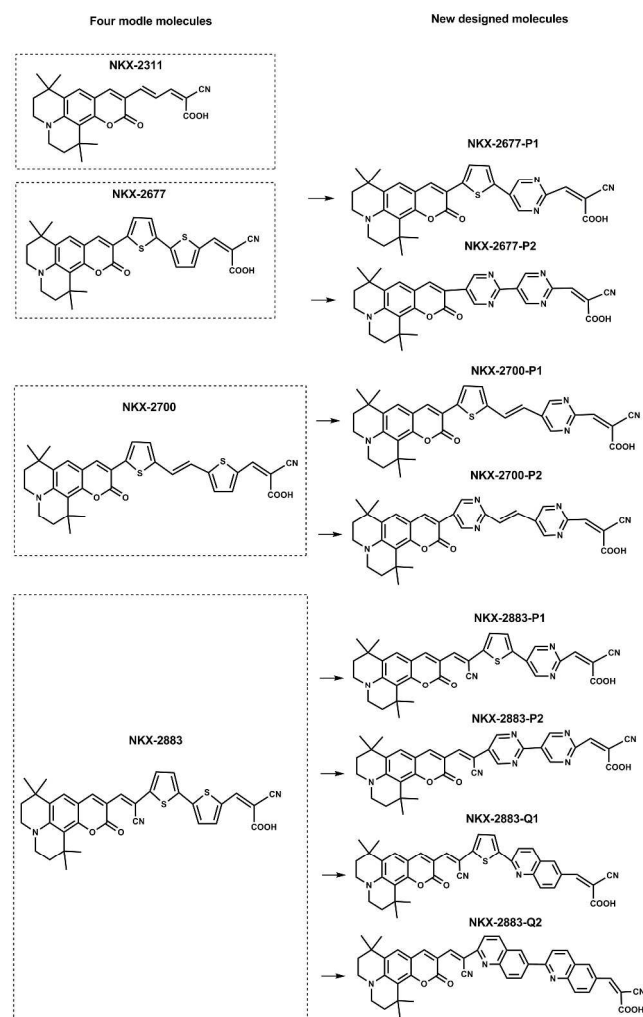


Fig.1 Chemical structure of twelve coumarin-based dyes

the performance of DSSCs with the related characters of ree dyes. Thus, the characters of dye/TiO₂ complexes should be probed to understand the electron transfer process from the dyes to TiO₂.

Herein, four model coumarin-derived chromophores (NKX-2311, NKX-2677, NKX-2700 and NKX-2883) were investigated to confirm the significant role of π -spacer in promoting the η of DSSCs (see Electronic Supplementary Information for detailed discussion). Then, different numbers of electron-deficient units (pyrimidine and quinoline) were adopted into NKX-2677, NKX-2700 and NKX-2883 to discuss the two questions mentioned above. The structures of all investigated dyes were illustrated in Fig. 1. To further rationalize the strategy presented in this work, eight dye/TiO₂ complexes were designed to investigate their geometrical and electronic structures, absorption spectra, electron injection efficiency.

We believe that the present effort to address the requirements of highly efficient DSSCs is a helpful exploration. The stimulated absorption spectra of NKX-2677, NKX-2700 and NKX-2883 reproduce the experimental results very well for the first time, indicating that the present theoretical methods are reliable. Compared with the three parent coumarin dyes, the new designed sensitizers have more outstanding

performance in optical absorption intensity and range. Generally, the strong spectral absorption does not always facilitate effectual charge separation, which means the performance of sensitizers is not only relied on the extrinsic spectral absorption intensity but also on the intrinsic character of electron movement upon photoexcitation. To assess the efficiency of charge separation, we apply a novel approach proposed by Le Bahers to quantify the charge transfer (CT) distance (L), the overlap (Ω) between the zones of density depletion and increment and the amount of transferred charge (Δe). The three parameters are evaluated only from the ground state (GS) and excited state (ES) total electronic densities. The central idea of this method is to compute the barycenters of the regions of increased/decreased of electronic densities. The results show that thorough charge-separation between the donor and the acceptor of sensitizers, and valid electron injection and regeneration can be gained by introducing electron-deficient units. Although the coumarin derivatives trigger intensive interest due to their application in DSSCs, as far as we know, theoretical studies on their dye/TiO₂ complexes still remain rather limited. Moreover, the electron injection mechanism will be influenced strongly by the electronic coupling (V) between dye molecule and semiconductor conduction band. Thus, it is necessary to give a deeper insight into the performance of dye/TiO₂ complexes, aiming to make sure the charge transfer and dye-TiO₂ interaction occurring at the semiconductor interface. In order to demonstrate how the electron-deficient modified π -bridge improve the performance of the DSSCs, comprehensive investigation, including electronic structures, absorption spectra and electron transfer for isolated coumarin dyes and dye/TiO₂ complexes, will be presented in the present work.

2. Computational details

All calculations were implemented using Gaussian 09 program. Firstly, we paid close attention to the selection of the most appropriate functional to get the vertical excitation energies and suitable HOMO and LUMO energy levels (HOMO is the highest occupied molecular orbitals and LUMO denotes the lowest unoccupied molecular orbitals) of dyes. The HOMO and LUMO levels of sensitizers were used to assess dye regeneration efficiency and electron injection efficiency. The ground-state geometry optimizations of four model compounds (NKX-2311, NKX-2677, NKX-2700 and NKX-2883) were performed in solvent ethanol using B3LYP/6-31G(d, p) level. The vertical excitation energies and energy levels of the four model systems were computationally explored using different functionals (including B3LYP, PBE0, CAM-B3LYP, LC-WPBE, M062X and WB97XD) and the results were compared with experiments. Calculations showed that the most suitable excitation energies were obtained by the M062X functional and the most fitting HOMO energy levels were got by the PBE0 functional (shown in Table 2S along with the experimental data). Besides, the dependencies of HOMO level and transition energy on molecular geometry were explored using the six functionals mentioned above, and it showed that the best results (listed in Table 2S and Table 3S) were obtained when ground-state geometries were optimized by the B3LYP functional. Therefore, for the eight newly designed coumarin

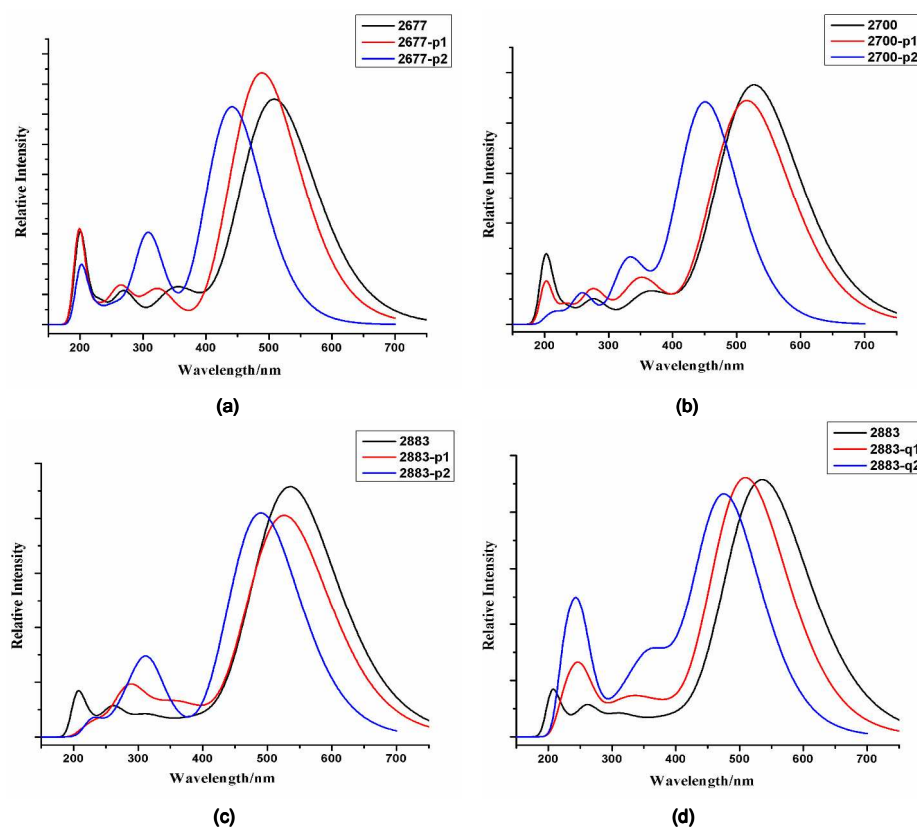


Fig.2 Calculated UV/Vis absorption spectra four series sensitizers in ethanol solution using M062X functional and the 6-31G(d,p) basis set (a) NKX-2677, NKX-2677-P1 and NKX-2677-P2; (b) NKX-2700, NKX-2700-P1 and NKX-2700-P2; (c) NKX-2883, NKX-2883-P1 and NKX-2883-P2; (d) NKX-2883, NKX-2883-Q1 and NKX-2883-Q2

dyes and the corresponding dye/TiO₂ complexes, their UV/VIS spectra and HOMO/LUMO levels were respectively calculated by the M062X and PBE0 functionals based on the B3LYP optimized geometries. Solvation is essential for accurate representation of molecules' excitation energies in the realistic environment, thus the solvent effect (in ethanol) was taken into account using the polarized continuum model (PCM) for all calculations.^{34, 35}

Then, the geometrical and electronic features of the free dyes were studied in detail. To investigate the efficiency of electron injection, both the compositions of those orbitals participated in the main electronic transitions and the driving force for electron injection were computed. The driving force for electron injection is related to the redox potentials which can be obtained by the Born-Haber cycle.³⁶ The Born-Haber cycle is connected with the geometrical optimization of the mono-valent and bi-valent oxidized coumarin sensitizers. All redox potentials involved in our study were obtained versus the normal hydrogen electrode (NHE). Furthermore, to assess the efficiency of charge separation, we computed the electron density difference of electron transitions. The electron densities of all orbitals related to the electron transitions were calculated with code Multwfn 2.5.³⁷ The extent of charge separation was quantified by the three parameters mentioned above, that is, the charge transfer distance (L), the overlap (Ω) between the zones of density depletion and increment, and the amount of transferred charge (Δe), which were calculated by DctViaCube software suit.²⁶

In order to study the dye-titania complexes, we selected a neutral, stoichiometric cluster of Ti₁₆O₃₂, by exposing anatase101 surface reported in Persson's work,³⁸ which is enough large to reproduce the electronic absorption spectra of the complexes. In this case a mixed basis set (standard LANL2DZ basis set for Ti atoms and 6-31G (d, p) basis set for C, N, S, H and O atoms) was used to perform geometry optimizations and TD-DFT calculations. Moreover, to evaluate the coupling interaction between dye and TiO₂ surface, the partial and total densities of states (PDOS and DOS) for the optimized complexes were investigated at the same theoretical level.

3. Results and discussion

The overall power conversion efficiency (η) can be characterized by the short-circuit current density (J_{sc}), the open circuit voltage (V_{oc}), and the fill factor of cell (FF), the η can be expressed as:²

$$\eta = \frac{J_{sc} \cdot V_{oc} \cdot FF}{P_{inc}} \quad (1)$$

where P_{inc} is the total solar power incident light on the solar cell, 100mW cm⁻² for AM 1.5. Correspondingly, J_{sc} is determined by the light-harvesting efficiency of dyes (ϕ_{LHE}), the efficiency of charge injection (ϕ_{inject}), the efficiencies of charge collection (ϕ_{cc}) and dye regeneration (ϕ_{reg}), it can be described by the following equation:³⁹

$$J_{sc} \propto \phi_{LHE} \cdot \phi_{cc} \cdot \phi_{inject} \cdot \phi_{reg} \quad (2)$$

In present work, we started discussion about the two question mentioned above from two aspects (J_{sc} (including ϕ_{LHE} , ϕ_{cc} , ϕ_{inject} and ϕ_{reg}) and V_{oc}).

3.1 How do different electron-deficient units and their number affect the performance of isolated dyes?

3.1.1 Adoption of single pyrimidine or quinoline unit

Firstly, single pyrimidine and quinoline units were adopted into model dyes to explore whether different electron-deficient units would have same effect on the efficiency of DSSCs. By comparing the performance of pyrimidyl-bridged and quinolyl-bridged dyes, we expect to identify which electron-deficient unit is more beneficial to improving η of coumarin-based DSSCs.

a. Absorption spectra

The simulated UV/VIS spectra of new designed dyes are presented in Fig. 2, and the related electronic transition data of all dyes are given in Table 4S. Apparently, all dyes exhibit two major absorption bands appearing at 400-600 nm (B1 band) and 200-400 nm (B2 band), respectively. The absorption band at 200-400 nm is ascribed to a localized π - π^* transition and the prominent band at 400-600 nm is attributed to the intramolecular charge transfer (ICT) excitation from donor to acceptor.

Calculated results shown that all the newly designed dyes with single electron-deficient unit exhibit a wider and stronger B2 (200-400 nm) band compared with the model sensitizers. The maximum absorption peaks (λ_{max}) and light capturing ability of dyes are almost unchanged with one electron-deficient unit adopted. Taking NKX-2677 and NKX-2677-P1 as example, for B1 band, the λ_{max} of NKX-2677-P1 is slightly blue-shifted by about 19 nm as compared with the reference dye NKX-2677.

Moreover, light-harvesting efficiency of NKX-2677 and NKX-2677-P1 are 0.986 and 0.991, respectively. Obviously, the slight blue shift and the almost unchanged light capturing ability indicate the photophysical properties in B1 band for coumarin dyes could be maintained with one electron-deficient unit adopted. For B2 band, the location of absorption peak (λ^*) for NKX-2677 is computed to be about 199 nm with oscillator strength $f=0.320$. In comparison with NKX-2677, the NKX-2677-P1 displays a quite stronger absorption band at 199 nm with $f=0.557$. Remarkably, the adoption of pyrimidine unit significantly enhances the absorption intensity of B2 band, and further increases the light-harvesting efficiency, ϕ_{LHE} (0.521 for NKX-2677 and 0.723 for NKX-2677-P1, as listed in Table 5S).

Accordingly, the adoption of electron-deficient unit greatly improves absorption properties in short-wavelength region with maintaining the intense absorption in long-wavelength region, which further increases the overall ϕ_{LHE} of dyes. Moreover, owing to stronger electron withdrawing ability, pyrimidine unit is more favorable to filling the optical absorption vacancy in short-wavelength region of coumarin sensitizers relative to quinoline unit.

b. Electronic structures and photoinduced charge transfer character

A favorable charge separation will facilitate electronic injection from excited dye to semiconductor surface, and then promote the photogenerated charge to be transported to the electrodes.² Consequently, effective electron collection efficiency

(ϕ_{cc}) requires a good intramolecular charge separation,⁴⁰ so we evaluated ϕ_{cc} with molecular orbital distribution and three parameters (L , Ω and Δe), respectively.²⁶

Generally, the sensitizers with push-pull structure are composed of an electron donor and an electron acceptor connected with conjugated π -spacer. In these systems, a photon absorption induces an electron transfer from the D part to the A part to form a $D^+-\pi-A^-$ excited state. Ideally, the electron completely transfers from the donor and localizes on the acceptor upon excitation. But in most real cases, the transferred charge is delocalized from the zone in the vicinity of the donor to region nearby the acceptor, which makes the extent of charge separation is different. For DSSCs, the η would be decreased due to the incomplete charge separation, so quantifying the length and magnitude of the CT is of much concern to evaluate the performance of sensitizer. In this work, three parameters of CT mentioned above are used to quantify the degree of electron transfer. The total electron densities of initial and final states and their centroids should be calculated.

The CT distance (L) is defined by two barycenters of the electronic density depletion (R_-) and increment (R_+) zones upon excitation.

$$L = |R_+ - R_-| \quad (3)$$

The barycenters of electronic density depletion (R_-) region and the electronic density increment (R_+) region associated with electronic transition should be defined by $\rho_+(r)$ and $\rho_-(r)$:

$$R_+ = (x_+, y_+, z_+) = \frac{\int_r \rho_+(r) dr}{\int \rho_+(r) dr} \quad (4)$$

and

$$R_- = (x_-, y_-, z_-) = \frac{\int_r \rho_-(r) dr}{\int \rho_-(r) dr} \quad (5)$$

To calculate the two barycenters, the increase $\rho_+(r)$ / decrease $\rho_-(r)$ of the density due to the electronic transition is expressed as:

$$\rho_+(r) = \begin{cases} \Delta\rho(r) & \text{if } \Delta\rho(r) > 0 \\ 0 & \text{if } \Delta\rho(r) < 0 \end{cases} \quad (6)$$

and

$$\rho_-(r) = \begin{cases} \Delta\rho(r) & \text{if } \Delta\rho(r) < 0 \\ 0 & \text{if } \Delta\rho(r) > 0 \end{cases} \quad (7)$$

In Equations (6) and (7), $\Delta\rho(r)$ is defined as:

$$\Delta\rho(r) = \rho^{ES}(r) - \rho^{GS}(r) \quad (8)$$

where $\rho^{ES}(r)$ and $\rho^{GS}(r)$ are the electronic densities associated to excited and ground states. The fraction of electron exchange can be expressed as:

$$\Delta e = \int \rho_+(r) dr = \int \rho_-(r) dr \quad (9)$$

The overlap (Ω) between the zones of density depletion and increment is written as:

$$\Omega \propto (L - H) \quad (10)$$

H is defined as half of the sum of the centroids axis (σ) along

Table 1 Frontier molecular orbital spatial distribution and electron density difference plots of electronic transition $S_0 \rightarrow S_1$ for each coumarin dyes performed in ethanol solution using the M062X functional with 6-31G(d,p) basis set. L is the electron transfer distance (\AA); Δe is the fraction of electron exchange (e^-), Ω is overlaps between the regions of density depletion and increment. (Isovalue: $4 \times 10^{-4} e^- \text{au}^{-3}$)

Molecule	HOMO	LUMO	picture	f	$L(\text{\AA})$	Δe	Ω
NKX-2311				1.774	5.164	1.024	0.376
NKX-2677				1.851	9.748	1.118	0.136
NKX-2677-P1				2.067	10.449	1.149	0.110
NKX-2677-P2				1.789	11.24	1.197	0.059
NKX-2700				2.347	10.995	1.060	0.143
NKX-2700-P1				2.194	11.841	1.166	0.076
NKX-2700-P2				2.178	12.812	1.155	0.052
NKX-2883				2.255	9.403	1.100	0.350
NKX-2883-P1				2.001	10.405	1.120	0.192
NKX-2883-P2				2.024	11.182	1.144	0.168
NKX-2883-Q1				2.270	11.782	1.050	0.216
NKX-2883-Q2				2.117	12.934	1.073	0.241

5 electron transfer direction.

To create an efficient charge-separated state, HOMO should be localized on the donor part, and LUMO should be localized on the acceptor.² From Table 1, the introduction of single electron-deficient unit changes the charge population of HOMOs from
 10 entire molecules to donor groups of sensitizers, which leads to effective charge-separated state for coumarin sensitizer. To illustrate visually the electron transition, the electron density difference plots of $S_0 \rightarrow S_1$ excitation and the three parameters were calculated (Table 1). In electron density difference plots, the
 15 direction of electron transfer is from the green area to the blue one. Clearly, the adoption of single pyrimidine or quinoline promotes more charge transfer to the acceptor part of dyes, and further increases the values of Δe and L , such as $1.100 e^-$ (NKX-2883) < $1.050 e^-$ (NKX-2883-Q1) < $1.120 e^-$ (NKX-2883-P1) and
 20 9.403\AA (NKX-2883) < 10.405\AA (NKX-2883-P1) < 11.782\AA (NKX-2883-Q1). It indicates that adding one pyrimidine or quinoline unit into dye contributes to the formation of effective charge-separated state. In addition, the overlap (Ω) between the zones of density depletion and increment is also an important
 25 parameter to determine whether an effective charge separation between the donor and acceptor occurs or not. The weak overlap

is accompanied by a good charge separation. As shown in Table 1, with one pyrimidine or quinoline adopted, the HOMO electron density of single electron-deficient unit tailored dyes is mainly
 30 localized on the coumarin343 moiety (the donor part), which decreases the values of overlap (Ω), the calculated overlap (Ω) complies with the order of $\Omega_{\text{NKX-2883-P1}}$ (0.192) < $\Omega_{\text{NKX-2883-Q1}}$ (0.216) < $\Omega_{\text{NKX-2883}}$ (0.350). Again, the present theoretical results suggested that the adoption of single electron-deficient unit
 35 (especially pyrimidine) is advantageous to the effective charge separation because of the weaker overlap.

c. Electron injection and regeneration for sensitizers

It is well known that the charge injection is one of the key electron transfer processes and is important for the performance
 40 of DSSCs devices.² In present work, we estimate the efficiency of electron injection from three aspects, that is, the energy levels of the acceptor fragment (conjugated π -spacer and anchoring group) and the donor of sensitizer, the electronic coupling between chromophores and TiO_2 surface, and driving force of electron
 45 injection.¹⁹ Also, dye regeneration is one of the most central electron transfer processes for the overall DSSCs performance in terms of both the reuse and long life expectancies of sensitizers. The regeneration efficiency can be evaluated by the driver force

Table 2 Calculated HOMO, LUMO energy levels (eV) of the donor (coumarin343), the acceptor (conjugated π -spacer and anchoring group) fragments and LUMO_{donor}-LUMO_{acceptor} of all sensitizer

molecule	ϵ_{LUMO}	ϵ_{HOMO}	$\epsilon_{\text{LUMOdonor-LUMOacceptor}}$
Coumarin343	-1.503	-5.512	
frag-2311	-2.665	-7.620	1.162
frag-2677	-2.807	-6.266	1.304
frag-2677-P1	-2.985	-6.842	1.482
frag-2677-P2	-3.110	-6.978	1.607
frag-2700	-2.839	-5.927	1.336
frag-2700-P1	-3.021	-6.364	1.518
frag-2700-P2	-3.108	-6.938	1.605
frag-2883	-3.004	-6.259	1.501
frag-2883-P1	-3.151	-6.757	1.648
frag-2883-P2	-3.229	-7.375	1.726
frag-2883-Q1	-3.022	-6.490	1.519
frag-2883-Q2	-2.966	-6.589	1.463

of dye regeneration. The driving forces depend strongly on the ground state oxidation potential of sensitizers ($E_{\text{ox(dye)}}$).¹⁹

$$E_{\text{ox(dye)}} \approx \epsilon_{\text{HOMO}} + 4.44 \text{ eV} \quad (11)$$

In this paper, all calculated results are gained by the PBE0 functional. The calculated (Table 2S) for NKX-2677, NKX-2700 and NKX-2883 are 0.900 eV, 0.810 eV and 1.022 eV, respectively. These results are well in agreement with the experimental values (0.91 eV for NKX-2677,²² 0.82 eV for NKX-2700²³ and 0.97 eV for NKX-2883).²⁴ The small discrepancy between theory and experiment (<0.1 eV) suggests that the present theoretical method is reliable.

In general, the electron transfer is described as that electron is supposed to move from the LUMO of coumarin to the LUMO of semiconductor tunneling through the LUMO of π -spacer.¹⁸ To estimate the efficiency of electron injection from dye to TiO₂ surface (ϕ_{inject}), the energy levels of donor fragment (coumarin 343) and acceptor moiety (conjugated π -spacer and anchoring group) were calculated (Table 2). Obviously, the LUMO energy levels of all of the acceptor groups are located below the LUMO energy level of C343 (-1.503 eV), which leads the energy drops of LUMO_{donor}-LUMO_{acceptor} for one-pyrimidine-bridged or one-quinoline-bridged dyes be larger than those of their parent analogues. It indicates that the introduction of electron-deficient unit is favorable for the charge transfer from C343 to acceptor (the π -spacer and anchoring group), and further increase the contributions from the anchoring group to LUMO of dyes (Table 3). As reported by Troisi *et al.*,⁴¹ the large contribution from anchoring group of dye to LUMO will effectively strengthen electronic coupling between sensitizer and conduction band of semiconductor. Strong electronic coupling^{42, 43} promotes the electron injection from dye to titania. From Table 3, our calculated results show that the contributions from the anchoring group of new designed dyes with single electron-deficient unit are comparatively larger than the corresponding reference dyes, which means the electronic coupling between dye and TiO₂ is effectively enhanced by modifying the π -spacer of coumarin dyes with electron-deficient units for efficient electron injection.

Additionally, the thermodynamic driving force (ΔG^0) for electron injection is an important parameter to characterize the efficiency of electron injection, which provides an evidence to

Table 3 Molecular orbital composition (in %) of the highest occupied and the lowest unoccupied molecular orbital of the twelve coumarin sensitizers performed in ethanol solvent using the M062X functional and the 6-31G(d,p) basis set

system	orbital	Anchoring ligand	π -linker	C343
NKX-2311	HOMO	11	12	77
	LUMO	35	20	46
NKX-2677	HOMO	4	34	62
	LUMO	39	49	12
NKX-2677-P1	HOMO	2	28	70
	LUMO	44	46	10
NKX-2677-P2	HOMO	0	8	92
	LUMO	48	47	4
NKX-2700	HOMO	3	43	54
	LUMO	35	56	9
NKX-2700-P1	HOMO	3	33	64
	LUMO	42	49	6
NKX-2700-P2	HOMO	0	10	90
	LUMO	45	55	3
NKX-2883	HOMO	3	39	58
	LUMO	24	56	19
NKX-2883-P1	HOMO	1	31	68
	LUMO	35	54	11
NKX-2883-P2	HOMO	0	19	80
	LUMO	41	52	7
NKX-2883-Q1	HOMO	1	34	65
	LUMO	34	56	10
NKX-2883-Q2	HOMO	0	24	76
	LUMO	42	54	4

screen promising sensitizers for DSSCs. The driving force can evaluate the electron injection efficiency related to the corresponding vertical excitation:¹⁸

$$\phi_{\text{inject}} \propto \Delta G^0 \quad (12)$$

and ΔG^0 can be calculated by the following equation:³⁶

$$\Delta G^0 = E_{\text{CB}} - \Delta E_{\text{ver}} - E_{\text{redox}} \quad (13)$$

where ΔE_{ver} represents the vertical excitation energy obtained from TD-DFT calculations. The value of E_{CB} is the conduction band edge of TiO₂ (-0.44V vs. NHE). ΔE_{redox} is the ground-state redox potentials of the studied system, which can be given by the Nernst equation.

Calculated driving forces of electron injection⁴³ for all sensitizers are also calculated and listed in Table 4. Introducing single pyrimidine or quinoline into dyes can increase the driving force, and further make for electron injection. For 2677 and NKX-2677-P1, the value of ΔG^0 for NKX-2677-P1 (-2.543 eV) is more negative than that of NKX-2677 (-2.290 eV), it suggests that introducing single pyrimidine into dyes can increase the driving force for electron injection, and further make for electron injection. As shown in Table 4, all the newly designed sensitizers with single electron-deficient units have more negative ΔG^0 than their corresponding parent compounds. Especially, both the electron injection driving forces of NKX-2883-P1 and NKX-2883-Q1 are more negative than that of NKX-2883 (the order is NKX-2883 (-2.210 eV) > NKX-2883-Q1 (-2.219 eV) > NKX-2883-P1 (-2.510 eV)). All results imply the introduction of single electron-deficient unit (especially pyrimidine unit) is conducive to improving the ϕ_{inject} of dyes.

The regeneration of sensitizers is also considered in the present

Table 4 Estimated ΔG_{aq} , ΔG^0 , ΔE_{ver} , $E_{\text{ox(dye)}}$, ΔG_{reg} , f and LHE for all coumarin sensitizers. All calculation is obtained by PBE0 functional with b-31g(d,p) basis set

scheme	ΔG_{aq}^a	ΔG^0^b	E_{redox}^c	ΔE_{ver}^d	$E_{\text{ox(dye)}}^e$	$E_{\text{ox(dye*)}}^f$	ΔG_{reg}^g	f^h	LHE^i
NKX-2311	10.302	-2.894	5.862	2.528	-1.131	-1.397	-0.831	1.626/ 0.345	0.976/0.548
NKX-2677	9.216	-2.290	4.776	2.047	-0.900	-1.147	-0.600	1.407/ 0.614	0.961/0.757
NKX-2677-P1	9.510	-2.543	5.070	2.087	-0.965	-1.123	-0.665	1.472/ 0.742	0.966/0.819
NKX-2677-P2	10.087	-3.070	5.647	2.138	-1.078	-1.059	-0.778	0.911/ 0.933	0.877/0.883
NKX-2700	8.890	-2.048	4.450	1.962	-0.810	-1.152	-0.510	1.825/ 0.710	0.985/0.805
NKX-2700-P1	9.241	-2.436	4.801	1.925	-0.896	-1.028	-0.596	1.575/ 0.891	0.973/0.872
NKX-2700-P2	9.674	-2.704	5.234	2.089	-1.055	-1.034	-0.755	1.080/ 1.305	0.917/0.951
NKX-2883	9.089	-2.210	4.649	1.998	-1.022	-0.976	-0.722	1.900/ 0.361	0.987/0.564
NKX-2883-P1	9.380	-2.510	4.940	1.990	-1.054	-0.936	-0.754	1.568/ 0.501	0.973/0.685
NKX-2883-P2	9.891	-2.889	5.451	2.122	-1.179	-0.944	-0.879	1.371/ 0.653	0.957/0.778
NKX-2883-Q1	9.140	-2.219	4.700	2.042	-1.046	-0.995	-0.746	1.695/ 0.577	0.980/0.735
NKX-2883-Q2	9.192	-2.068	4.752	2.244	-1.099	-1.145	-0.799	1.430/ 0.668	0.963/0.785

^a Calculated Gibbs free energy change (ΔG_{aq} , in V) due to the oxidation of the dyes in aqueous solutions. ^b The driving force (ΔG^0 , in V) electron injection related to the electronic transition in B1 band. ^c Redox potential (E_{redox} vs NHE, in V). ^d The vertical excitation energy (ΔE_{ver} , eV) corresponding to the maximum wavelength of spectral absorption. ^e The oxidized potential (vs. NHE, $E_{\text{ox(dye)}}$, in eV) of ground state. ^f The oxidized potential of the first excited state ($E_{\text{ox(dye*)}}$) following unrelax path for dyes. ^g The regeneration energy (ΔG_{reg} , in V). ^h The oscillation strength of the two major absorption bands (B1 and B2 bands). ⁱ The light harvest efficiency (LHE) corresponding to B1/B2 bands. Here the NHE is declared to be zero at all temperatures and its Gibbs free energy change takes the standard value of -4.44 eV.

research, and it can be estimated by the driver force of dye regeneration (ΔG_{reg}).¹⁸

$$\Delta G_{\text{reg}} = E_{\text{ox(dye)}} + 0.3 \quad (14)$$

As listed in Table 4, the regeneration driving forces are NKX-2677 (-0.600 eV) > NKX-2677-P1 (-0.665 eV) and NKX-2700 (-0.510 eV) > NKX-2700-P1 (-0.596 eV), indicating that the adoption of single pyrimidine unit is beneficial to the dye regeneration. For NKX-2883-P1 and 2883-Q1, the values of regeneration driving forces also become more negative with the introduction of electron-deficient unit and the order of driving force for dye regeneration is NKX-2883 (-0.722 eV) > NKX-2883-Q1 (-0.746 eV) > NKX-2883-P2 (-0.754 eV). All calculated results imply the driving forces for dye regeneration should be more negative by adopting electron-deficient unit (see Table 4).

d. The open circuit voltage

For our investigated dyes, the adoption of electron-deficient unit slightly affects the shift of conduction band edge of semiconductor, so the number of injected electron in the conduction band (n_c) is the main factor that influence the values of V_{oc} . As reported by Kusama *et al.*,⁴⁴ injected electron in conduction band of TiO₂ could recombine with electron acceptor (I_2) and oxidized sensitizers leading to small n_c . It is accepted that I_2 preferred to bind with N of CN, S of thiophene forming dye-iodine complexes available for serious charge recombination, which is the main route of photovoltage losses.^{16, 45} In this work, the absence of sulfur atom in electron-deficient unit (pyrimidine and quinoline) for NKX-2677-P1, NKX-2700-P1, NKX-2883-P1 and NKX-2883-Q1 could be beneficial to suppress charge recombination, which improves the n_c for high V_{oc} .

3.1.2 Introduction of a couple of pyrimidine or quinoline units

Secondly, a second pyrimidine or quinoline unit was adopted into single electron-deficient unit tailored dyes to explore the quantity of electron-deficient unit how to affect the properties of dyes.

a. Absorption spectra

Similarly, the UV-VIS absorption spectra of NKX-2677-P2, NKX-2700-P2, NKX-2883-P2 and NKX-2883-Q2 also exhibit two major absorption (B1 and B2) bands. The maximum

absorption peak (λ_{max}) of NKX-2677-P2 adopted the second pyrimidine unit blue-shifts to 441 nm from 489 nm of NKX-2677-P1 (see Table 4S) which could be explained by the fact that the dihedral angle formed between the π -spacer and coumarin343 of NKX-2677-P2 is more than 10°, whereas the dihedral angle of NKX-2677-P1 is less than 3°. NKX-2677-P2 displays a stronger and red-shifted B2 absorption band (λ^*) comparing with NKX-2677-P1. As shown in Table 4S, the M062X functional simulated B2 band is red-shifted with inserting a second pyrimidine moiety from NKX-2677-P1 to NKX-2677-P2 by 102 nm, and their corresponding oscillation strengths are 0.557 and 0.678, respectively. Thus, the calculated ϕ_{LHE} of B2 band increases with the growing number of pyrimidine unit (0.723 for NKX-2677-P1 and 0.790 for NKX-2677-P2). Obviously, the two pyrimidine or quinoline units in these four dyes destroy the planarity of molecular backbone, which results in a significant blue-shifted B1 band. However, the situation of B2 band is just opposite to that of B1 band, that is, the introduction of a couple of pyrimidine or quinoline units effectively shifts the absorption peaks (λ^*) of B2 band to longer wavelength region and significantly enhances the corresponding absorption intensity. Comprehensively, we considered that increasing the amount of electron-deficient units is unfavorable for improving the ϕ_{LHE} of coumarin dye due to the obviously blue shift of λ_{max} .

b. Electronic structures and photoinduced charge transfer character

As shown in Table 1, the electron density distributions of HOMOs of the sensitizers with two electron-deficient groups are more centralized on the coumarin343 than that of the dyes with single electron-deficient units, whereas all the sensitizers' LUMOs are localized on the linker and acceptor moieties. This reveals that the introduction of two electron-deficient units changes the charge population of HOMOs and induces the better charge separation. Also, the three important parameters (L , Δe and Ω) of CT are calculated and used to discuss the property of charge transfer for the new sensitizers. Our calculated results show that with increase of the number of electron-deficient pyrimidine the values of Δe and L are raised, whereas the value of the overlap is decreased. This means that the increase of

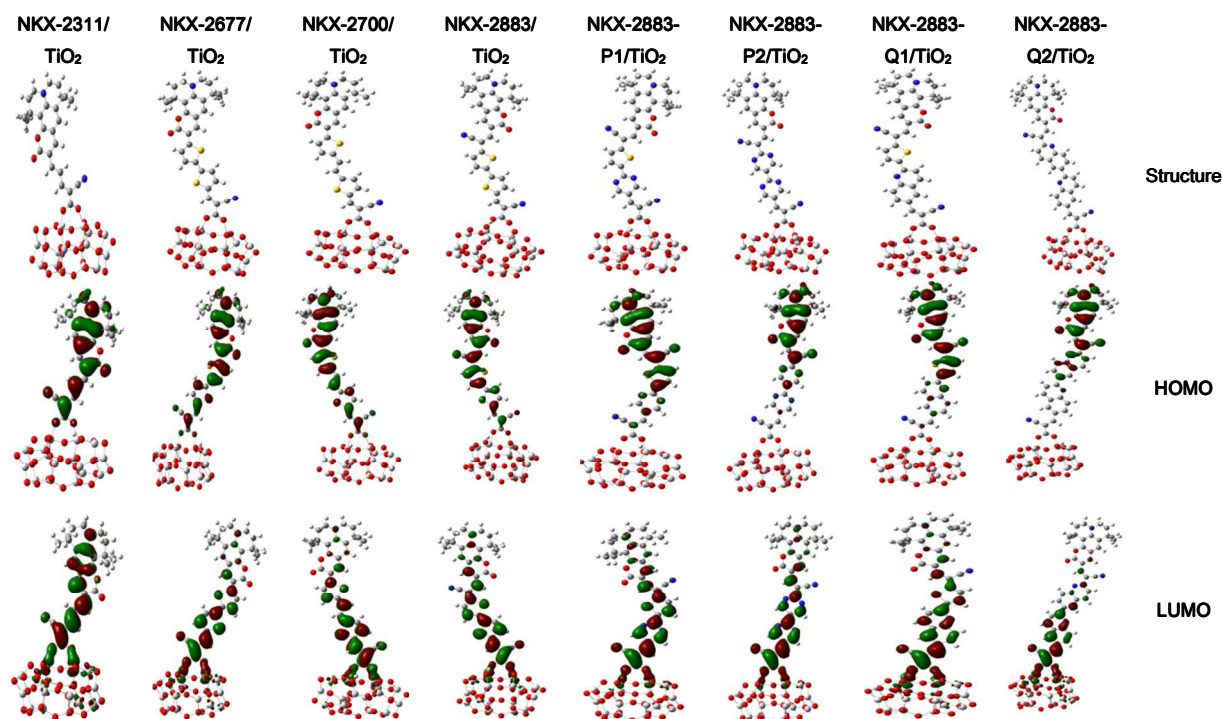


Fig 3. Optimized geometries for the eight dye/TiO₂ complexes and their HOMO and LUMO orbitals relevant during photoexcitation

pyrimidine would be helpful to improve the efficiency of charge separation. However, the overlap of NKX-2883-Q2 is larger than that of NKX-2883-Q1 (although they are still smaller than that of NKX-2883, the order is $\Omega_{\text{NKX-2883-Q1}} (0.2162) < \Omega_{\text{NKX-2883-Q2}} (0.2410) < \Omega_{\text{NKX-2883}} (0.3495)$, which indicates the adoption of single quinoline favors charge separation, but the introduction of couple of quinoline units could not further improve the efficiency of charge separation. Thus, the increasing number of quinoline is not suitable to improve the performance of coumarin-based DSSCs. The reason that pyrimidine unit motivates more effective charge separation than quinoline group may come from the following facts: better coplanarity of pyrimidine with their neighboring groups and its stronger electron withdrawing ability.

c. Electron injection and regeneration for sensitizers

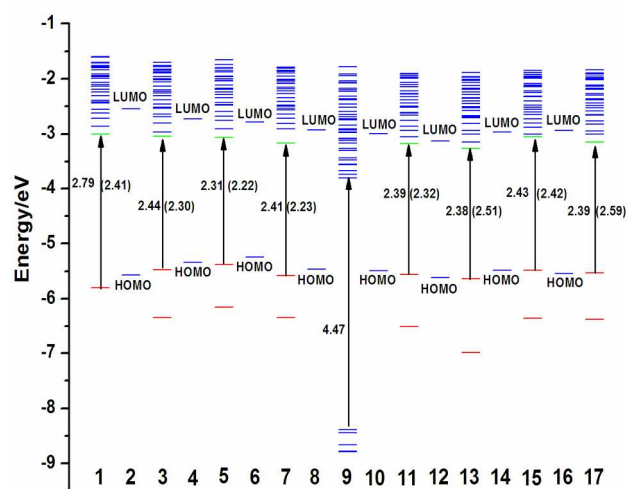
From Table 2, evidently, the LUMO energy levels of all the acceptor groups with two pyrimidine units are located below those of all the acceptor moieties with single pyrimidine, therefore the energy drop of LUMO_{donor}-LUMO_{acceptor} would be effectively increased with more pyrimidine unit adopted. It suggests that the adoption of more pyrimidine units is favorable for charge separation between the C343 donor and the extended acceptor (the π -spacer and anchoring group) and further increases the contribution from the anchoring group to the LUMO of dye (Table 3). For example, the contributions for NKX-2883-P1 and NKX-2883-P2 respectively are 35% and 41%, which indicates that NKX-2883-P2 has stronger electronic coupling between sensitizers and TiO₂ surface for effective electron injection. Also, as shown in Table 4, the more the adopted pyrimidine units, the higher the driving force of electron injection would be. However, due to the weaker electron withdrawing ability of quinoline unit and poor coplanarity of multiple quinoline-bridged dyes, it should be pointed out that the energy drop of 2883-Q2 (1.436 eV) is

slightly smaller than that of 2883-Q1 (1.459 eV) and the values of $\Delta G_{(\text{dye})}^0$ become more negative with more quinoline introduced into coumarin dyes (-2.219 eV (NKX-2883-Q1) > -2.068 eV (NKX-2883-Q2)), which implies the introduction of more quinoline units weakens the charge separation and is not conducive to the electron injection process.

The driving force of dye regeneration (ΔG_{reg}) is also calculated and is used to investigate the relationship between the amount of electron-deficient units and the efficiency of dye regeneration. As displayed in Table 4, the absolute values of driving forces for dye regeneration are increased with more pyrimidine or quinoline unit adopted, which means that increasing the amount of pyrimidine and quinoline units could promote the regeneration of oxidized dyes.^{46, 47} The effective regeneration of oxidized dyes is beneficial to the unidirectional charge transport and avoiding the charge recombination.⁴⁸ Alebbi⁴⁹ pointed out that inefficient regeneration could limit the device photocurrent. Therefore, the present theoretical results reveal that the sensitizers combining two electron-deficient groups should have a vantage of regeneration of oxidized dyes.

3.2 How do different electron-deficient units and their number affect electronic structures and absorption spectra of dye-TiO₂ complexes?

So far, we have described how the electron-deficient units and their number affect the electronic and structural properties of free coumarin sensitizers, but it is not sufficient to look at the electronic structures of these systems individually. Thus, the next step in this contribution was to investigate the dye/titania complexes^{2, 15, 50} (including their electronic structures, absorption spectra, and electronic coupling between dye and TiO₂). FT-IR^{8, 18} study suggested that the sensitizers are chemically adsorbed on the surface of nanocrystalline TiO₂ in a bidentate carboxylate



mode. In this bidentate structure, both the carboxylic oxygen atoms are bound to two five-fold coordinated Ti atoms, and the

Fig.4 Molecular orbital energy level (eV) diagram of (column 1) 2311/TiO₂ complex, (column 2) NKX-2311 dye, (column 3) 2677/TiO₂ complex, (column 4) NKX-2677 dye, (column 5) 2700/TiO₂ complex, (column 6) NKX-2700, (column 7) 2883/TiO₂ complex, (column 8) NKX-2883 dye, (column 9) isolated TiO₂, (column 10) NKX-2883-P1 dye, (column 11) 2883-P1/TiO₂ complex, (column 12) NKX-2883-P2 dye, (column 13) 2883-P2/TiO₂ complex, (column 14) NKX-2883-Q1 dye, (column 15) NKX-2883-Q1/TiO₂ complex, (column 16) NKX-2883-Q2 dye and (column 17) 2883-Q2/TiO₂ complex in ethanol solution. Green represents localization of molecular orbital both on the dye and the surface. Blue represents localization of molecular orbital on TiO₂. Red represents localization of molecular orbital on dyes.

acid hydrogen atom (H) is bound to the bridging oxygen on the TiO₂ surface. Therefore we adopted the bidentate bridging mode for adsorption of all of the sensitizers on the TiO₂ nanoparticle surface. The optimized geometries for the four dye/TiO₂ complexes are given in Fig. 3. Generally, upon excitation, charge injection from sensitizer to semiconductor can occur through direct mechanism or indirect mechanism.^{50, 51} The direct mechanism is a “one-step” electron injection from the ground state of sensitizer to the conduction band of semiconductor. In the direct-mechanism case, a new charge-transfer band should appear in the absorption spectrum, but it is not present in the spectra of isolated sensitizer and semiconductor. In indirect mechanism, the charge is firstly provoked from the ground state of sensitizer to excited state which is also localized on dye itself, and then the charge transfers from excited state into the conduction band. The mechanism of electron injection plays a vital role in determining η of DSSCs. In the following discussion, we focused on these five dye/TiO₂ complexes (including NKX-2883/TiO₂, NKX-2883-P1/TiO₂, NKX-2883-P2/TiO₂, NKX-2883-Q1/TiO₂ and NKX-2883-Q2/TiO₂ complexes) to probe how the different electron-deficient units and their number affect the performance of these newly designed dye-titania complexes.

For all dye/TiO₂ complexes, the absorption properties are closely related to those of their free dyes. As presented in Figs. 1S-3S, it is found that a broad and enhanced B2 absorption is obtained for all the dye-titania complexes with single electron-deficient unit, which fills the optical absorption vacancy in short-wavelength region and thus improves the photo-to-electric

efficiency of coumarin-based DSSCs. While for those dye/TiO₂ complexes with two electron-deficient groups, the efficiency is not significantly enhanced due to the seriously blue-shifted absorption in long-wavelength region, although the oscillator strength of B2 band is also strengthened.

Several photo-excitations are involved in the formation of absorption spectra of these five complexes. A few of these excitations showing high oscillator strengths are given in Table 4S. Most of these excitations are mainly originated from HOMO to HOMO-2. The unoccupied orbitals involved in the major excitations mainly come from LUMO (Table 4S). For these five complexes, the change in electronic structure upon adsorption is small, which results in the energy of isolated photoexcited dyes to reside near the energy of excited states of dye-titania complexes. Thus, LUMOs of dye-titania complexes are very similar to those of free dyes, and therefore localized mainly on dyes, which means weak electronic coupling between dyes and TiO₂.² As reported in previous literature,¹⁵ the electronic coupling between semiconductor conduction band and dye molecule strongly influences the electron injection mechanism. The direct mechanism requires a strong electronic coupling, while weak electronic coupling favors the indirect mechanism. It suggests that in the present cases the indirect mechanism should be more possible. Besides, the different number of pyrimidine and quinoline units only has a small effect on the electronic structures of these dye-titania complexes.

After binding to titanium there is a redistribution of energy levels.³⁹ The computed Kohn-Sham orbital energy levels for isolated dyes, (TiO₂)₁₆ cluster and dye/TiO₂ complexes are presented in Fig. 4. As reported in previous studies, the higher the LUMO is located in the semiconductor conduction band, the more efficient the electron injection is. From Fig. 4, LUMOs of NKX-2883-P1/TiO₂ and NKX-2883-Q1/TiO₂ are localized higher than that of NKX-2883/TiO₂, which implies the introduction of single pyrimidine or quinoline unit contributes to providing more sufficient driving force for electron injection. However, compared with NKX-2883-P1/TiO₂ complex, the location of LUMO for NKX-2883-P2/TiO₂ complex is almost unchanged, revealing that they have almost the same electron injection efficiency. Introducing one more quinoline unit into NKX-2883-Q1/TiO₂ makes the location of LUMO for NKX-2883-Q2/TiO₂ is lower, and therefore decreases the efficiency of electron injection, which accords with our discussed results mentioned above. To better predict the efficiency of electron injection, we should adopt the molecular dynamics of the ultrafast electron injection in our further research.⁵²⁻⁵⁴

The total and partial densities of states¹⁸ for dye/TiO₂ complexes were used to illustrate electronic coupling between the dye and cluster, which are showed in Fig. 4S. For all dye-titania complexes, the electronic densities of LUMO orbitals are mainly localized on the dyes with slight contribution on cluster, it suggests weak electronic coupling between dye and TiO₂. This small contribution plays a key role in heterogeneous electron transfer. From Fig. 4S, we clearly observe that with single pyrimidine and quinoline units adopted into NKX-2883/TiO₂ complex, this small contribution is increased slightly, which indicates more mixing between dye and cluster orbitals leading to slightly enhanced electron coupling between dye and TiO₂. With

one more pyrimidine or quinoline units adopted into NKX-2883-P1/TiO₂ and NKX-2883-Q1/TiO₂ complexes, the contributions from the cluster to unoccupied molecular orbitals is almost unaltered, it implies the interfacial interaction between dye and TiO₂ cluster would be insensitive by increasing the number of pyrimidine or quinoline units.

In the present work, only two pyrimidine and quinoline units are used to study the number of electron-deficient units how to influences the performance of sensitizers and DSSCs. We believe it is enough because it has been found that the introduction of two electron-deficient units seems unfavorable for improving the photophysical properties of dye/TiO₂ systems. Additionally, in our previous report,¹⁹ we have proved that the extension the length of the π -spacer is disadvantageous to increase the performance of DSSCs.

4. Conclusions

In summary, we offered a comprehensive discussion about the influence of different electron-deficient units and their amount on absorption property, charge separation, electron injection and dye regeneration. Briefly, the J_{sc} (ϕ_{LHE} , ϕ_{cc} , ϕ_{inject} and ϕ_{reg}) and V_{oc} can be effectively improved by adopting single pyrimidine or quinoline unit into model coumarin dyes. Moreover, owing better coplanarity with the neighboring groups and its stronger electron withdrawing ability, pyrimidine should be more suitable to improve the performance of DSSCs relative to quinoline. Further, with a second electron-deficient unit adopted, a red-shifted and strengthened absorption in short-wavelength region and a blue-shifted absorption in long-wavelength region are obtained. The introduction of more pyrimidine units facilitates the electron transfer from donor to acceptor and favors the effective electron injection, whereas the second quinoline displays opposite effect. Despite the introduction of electron-deficient unit makes for electronic coupling between dyes and TiO₂, but cannot alter the indirect mechanism of electron injection for these investigated systems. The present theoretical exploration shows that the performance of metal-free coumarin sensitizers and the efficiency of the DSSCs are sensitive to the amount and variety of electron-deficient units. We believe it is a promising future research direction to broaden and strengthen the absorption in short-wavelength region (B band) of metal-free coumarin sensitizer and further improve the efficiency of the DSSCs.

Acknowledgements

We acknowledge generous financial support from the National Natural Science Foundation of China (Nos.21173169 and 20803059), Chongqing Municipal Natural Science Foundation (cstc2013jcyjA90015) and the Fundamental Research Funds for the Central Universities (No.DXJK2013A008)

Notes and references

^a School of Chemistry and Chemical Engineering, Southwest University, Chongqing 400715, China; E-mail: herx@swu.edu.cn

^b Education Ministry Key Laboratory on Luminescence and Real-Time Analysis, Southwest University, Chongqing 400715, China

^c Department of Applied Chemistry, Institute of Molecular Science and Center for Interdisciplinary Molecular Science, National Chia-Tung University, Hsinchu 300, Taiwan

†Electronic Supplementary Information (ESI) available: [Detailed discussion and calculated results obtained by different functionals (BLYP, PBE0 or M062X)]. See DOI: 10.1039/b000000x/

1. B. O'regan and M. Grätzel, *nature*, 1991, **353**, 737-740.
2. A. Hagfeldt, G. Boschloo, L. Sun, L. Kloo and H. Pettersson, *Chem. Rev.*, 2010, **110**, 6595-6663.
3. M. Grätzel, *J. Photochem. Photobio., C*, 2003, **4**, 145-153.
4. M. Grätzel, *J. Photochem. Photobio., A*, 2004, **164**, 3-14.
5. M. K. Nazeeruddin, F. De Angelis, S. Fantacci, A. Selloni, G. Viscardi, P. Liska, S. Ito, B. Takeru and M. Grätzel, *J. Am. Chem. Soc.*, 2005, **127**, 16835-16847.
6. N. Martsinovich and A. Troisi, *Energ. Environ. Sci.*, 2011, **4**, 4473-4495.
7. R. R. Frontiera, J. Dasgupta and R. A. Mathies, *J. Am. Chem. Soc.*, 2009, **131**, 15630-15632.
8. S. Agrawal, P. Dev, N. J. English, K. R. Thampi and J. MacElroy, *J. Mater. Chem.*, 2011, **21**, 11101-11108.
9. G. Reynolds and K. Drexhage, *Opt. Commun.*, 1975, **13**, 222-225.
10. R. Sánchez-de-Armas, M. Á. San Miguel, J. Oviedo and J. F. Sanz, *Phys. Chem. Chem. Phys.*, 2012, **14**, 225-233.
11. A. Yella, H.-W. Lee, H. N. Tsao, C. Yi, A. K. Chandiran, M. K. Nazeeruddin, E. W.-G. Diao, C.-Y. Yeh, S. M. Zakeeruddin and M. Grätzel, *Science*, 2011, **334**, 629-634.
12. K. Hara, T. Sato, R. Katoh, A. Furube, Y. Ohga, A. Shinpo, S. Suga, K. Sayama, H. Sugihara and H. Arakawa, *J. Phys. Chem. B*, 2003, **107**, 597-606.
13. Z.-S. Wang, Y. Cui, Y. Dan-oh, C. Kasada, A. Shinpo and K. Hara, *J. Phys. Chem. C*, 2008, **112**, 17011-17017.
14. X. Zhang, J.-J. Zhang and Y.-Y. Xia, *J. Photochem. Photobio., A*, 2008, **194**, 167-172.
15. R. Sánchez-de-Armas, M. A. San-Miguel, J. Oviedo and J. F. Sanz, *J. Chem. Phys.*, 2012, **136**, 194702.
16. Y. Wu and W. Zhu, *Chem. Soc. Rev.*, 2013, **42**, 2039-2058.
17. L.-Y. Lin, C.-H. Tsai, K.-T. Wong, T.-W. Huang, C.-C. Wu, S.-H. Chou, F. Lin, S.-H. Chen and A.-I. Tsai, *J. Mater. Chem.*, 2011, **21**, 5950-5958.
18. M. Guo, R. He, Y. Dai, W. Shen, M. Li, C. Zhu and S. H. Lin, *J. Phys. Chem. C*, 2012, **116** (16), 9166-9179
19. M. Guo, M. Li, Y. Dai, W. Shen, J. Peng, C. Y. Zhu, S. H. Lin and R. X. He, *RSC Adv.*, 2013, **3**, 17515-17526.
20. K. Hara, Z.-S. Wang, T. Sato, A. Furube, R. Katoh, H. Sugihara, Y. Dan-oh, C. Kasada, A. Shinpo and S. Suga, *J. Phys. Chem. B*, 2005, **109**, 15476-15482.
21. X. Ren, Q. Feng, G. Zhou, C.-H. Huang and Z.-S. Wang, *J. Phys. Chem. C*, 2010, **114**, 7190-7195.
22. K. Hara, Y. Dan-oh, C. Kasada, Y. Ohga, A. Shinpo, S. Suga, K. Sayama and H. Arakawa, *Langmuir*, 2004, **20**, 4205-4210.
23. Z.-S. Wang, Y. Cui, Y. Dan-oh, C. Kasada, A. Shinpo and K. Hara, *J. Phys. Chem. C*, 2007, **111**, 7224-7230.
24. Z. S. Wang, Y. Cui, K. Hara, Y. Dan - oh, C. Kasada and A. Shinpo, *Adv. Mater.*, 2007, **19**, 1138-1141.
25. H. Choi, H. Choi, S. Paek, K. Song, M.-s. Kang, J. Ko, *Bull. Korean Chem. Soc.*, 2010, **31**, 125-132.
26. I. Ciofini, T. Le Bahers, C. Adamo, F. Odobel and D. Jacquemin, *J. Phys. Chem. C*, 2012, **116**, 11946-11955.
27. T. Le Bahers, C. Adamo and I. Ciofini, *J. Chem. Theory Comput.*, 2011, **7**, 2498-2506.

28. M. J. Frisch, G. W. Trucks, H. B. Schlegel, G. E. Scuseria, M. A. Robb, J. R. Cheeseman, G. Scalmani, V. Barone, B. Mennucci, G. A. Petersson, H. Nakatsuji, *et al.*, *Gaussian 09, Revision A.01*, Gaussian, Inc., Wallingford, CT, 2009.
- 50 J. Preat, C. Michaux, D. JacquemiH. Nakatsuji, Gaussian 09, Gaussian Inc., Wallingford CT, Revision A.01 edn, 2009
29. Y. Kurashige, T. Nakajima, S. Kurashige, K. Hirao and Y. Nishikitani, *J. Phys. Chem. A*, 2007, **111**, 5544-5548.
30. T. Le Bahers, F. Labat, T. Pauporté, P. P. Lainé and I. Ciofini, *J. Am. Chem. Soc.*, 2011, **133**, 8005-8013.
- 10 31. P. Dev, S. Agrawal and N. J. English, *J. Phys. Chem. A*, 2013, **117**, 2114-2124.
32. I. H. Nayyar, E. R. Batista, S. Tretiak, A. Saxena, D. L. Smith and R. L. Martin, *J. Chem. Theory Comput.*, 2013, **9**, 1144-1154.
- 15 33. F. Lachaud, C. Jeandon, M. Beley, R. Ruppert, P. C. Gros, A. Monari and X. Assfeld, *The Journal of Physical Chemistry A*, 2012, **116**, 10736-10744.
34. D. Maftai, G. Zbancioc, I. Humelnicu and I. Mangalagiu, *J. Phys. Chem. A*, 2013, **117**, 3165-3175.
- 20 35. F. Lipparini and V. Barone, *J. Chem. Theory Comput.*, 2011, **7**, 3711-3724.
36. J. Wang, F.-Q. Bai, B.-H. Xia, L. Feng, H.-X. Zhang and Q.-J. Pan, *Phys. Chem. Chem. Phys.*, 2011, **13**, 2206-2213.
37. T. Lu and F. Chen, *J. Chem. Theory Comput.*, 2012, **33**, 580-592.
- 25 38. M. Nilsing, P. Persson and L. Ojamäe, *Chem. Phys. Lett.*, 2005, **415**, 375-380.
39. A. V. Akimov, A. J. Neukirch and O. V. Prezhdo, *Chem. Rev.* 2013, **113**, 4496-4565.
40. S. Nachimuthu, C.-M. Lo and J.-C. Jiang, *J. Phys. Chem. Lett.*, 2013, **4**, 524-530.
- 30 41. D. R. Jones and A. Troisi, *Phys. Chem. Chem. Phys.*, 2010, **12**, 4625-4634.
- 65 42. M. Pastore and F. D. Angelis, *ACS nano*, 2009, **4**, 556-562.
43. J. M. Rehm, G. L. McLendon, Y. Nagasawa, K. Yoshihara, J. Moser and M. Grätzel, *J. Phys. Chem.*, 1996, **100**, 9577-9578.
- 35 44. H. Kusama and H. Sugihara, *J. Comput. Chem.*, 2005, **26**, 1372-1382.
45. W. Li, Y. Wu, Q. Zhang, H. Tian and W. Zhu, *ACS Appl. Mater. Interfaces*, 2012, **4**, 1822-1830.
46. S. M. Feldt, P. W. Lohse, F. Kessler, M. K. Nazeeruddin, M. Grätzel, G. Boschloo and A. Hagfeldt, *Phys. Chem. Chem. Phys.*, 2013.
- 40 47. T. Daeneke, A. J. Mozer, T.-H. Kwon, N. W. Duffy, A. B. Holmes, U. Bach and L. Spiccia, *Energ. Environ. Sci.*, 2012, **5**, 7090-7099.
48. J. N. Clifford, E. Palomares, M. K. Nazeeruddin, M. Grätzel, J. Nelson, X. Li, N. J. Long and J. R. Durrant, *J. Am. Chem. Soc.*, 2004, **126**, 5225-5233.
- 45 49. M. Alebbi, C. A. Bignozzi, T. A. Heimer, G. M. Hasselmann and G. J. Meyer, *J. Phys. Chem. B*, 1998, **102**, 7577-7581.
50. S. Agrawal, P. Dev, N. J. English, K. R. Thampi and J. MacElroy, *Chem Sci*, 2012, **3**, 416-424.
- 50 51. R. o. Sánchez-de-Armas, J. Oviedo, M. A. n. San Miguel and J. F. Sanz, *J. Phys. Chem. C*, 2011, **115**, 11293-11301.
52. R. Long and O. V. Prezhdo, *J. Am. Chem. Soc.*, 2011, **133**, 19240-19249.
- 55 53. D. P. Hoffman, O. P. Lee, J. E. Millstone, M. S. Chen, T. A. Su, M. Creelman, J. M. Frechet and R. A. Mathies, *J. Phys. Chem. C*, 2013, **117**, 6990-6997
54. A. Listorti, B. O'Regan and J. R. Durrant, *J. Mater. Chem.*, 2011, **23**, 3381-3399.
- 60